GBE

Sex-Specific Landscapes of Crossover and Noncrossover Recombination in Coppery Titi Monkeys (*Plecturocebus cupreus*)

Cyril J. Versoza[1], Karen L. Bales[2,3,4], Jeffrey D. Jensen [1], Susanne P. Pfeifer [1,*]

[1]Center for Evolution and Medicine, School of Life Sciences, Arizona State University, Tempe, AZ, USA
[2]Department of Psychology, University of California, Davis, CA, USA
[3]California National Primate Research Center, Neuroscience and Behavior Division, Davis, CA, USA
[4]Department of Neurobiology, Physiology, and Behavior, University of California, Davis, CA, USA

*Corresponding author: E-mail: susanne@spfeiferlab.org.

Accepted: July 14, 2026

Abstract

Along with germline mutations, meiotic recombination plays a fundamental role in shaping genetic diversity and thus directly influences a species' potential adaptive response to environmental change, amongst other features. Despite the recombination landscape being of central importance for a variety of questions in molecular evolution, the genome-wide distribution and frequency of recombination remains to be elucidated in many nonhuman primate species. Utilizing novel high-coverage genomic data from three multi-sibling families, we here provide the first estimates of the rates and patterns of crossover and noncrossover recombination in coppery titi monkeys (*Plecturocebus cupreus*)—a socially monogamous, pair-bonded primate that serves as an important model in behavioral research. Consistent with haplorrhines, crossover and noncrossover recombination in this platyrrhine are frequently localized at PRDM9-mediated hotspots, characterized by a 15-mer binding motif with substantial similarities to the degenerate 13-mer motif found in humans. The sex-averaged crossover rate in coppery titi monkeys is comparable with those of other primates; however, no significant difference in recombination rates was observed between the sexes, despite a pronounced maternal age effect in the species. Similarities also exist with regards to the sex-specific genomic distribution of noncrossover events, though the minimal conversion tract lengths of extended events was observed to be considerably longer in maternally inherited noncrossovers. Taken together, these similarities and differences in the recombination landscape relative to other primates highlight the importance of incorporating species-specific rates and patterns in evolutionary models, and the resources provided here will thus serve to aid future studies in this important primate model system.

Key words: recombination, primate, platyrrhine, Pitheciidae, population genomics.

Significance

Meiotic recombination plays a fundamental role in shaping population genetic diversity. Utilizing whole genome data from three multi-sibling families, we here provide the first estimates of the rates and patterns of crossover and noncrossover recombination in coppery titi monkeys (*Plecturocebus cupreus*)—a socially monogamous, pair-bonded primate that serves as an important model in behavioral research.

Introduction

Along with germline mutations, meiotic recombination plays a fundamental role in generating and shaping observed genetic diversity (see the review of Johnston 2024). A requisite for the faithful segregation of homologous chromosomes during gametogenesis (Keeney 2001), recombination in primates is thought to primarily take place at PRDM9-mediated hotspots (Baudat et al. 2010; Myers et al. 2010; Parvanov et al. 2010). Localizing these hotspots by binding DNA at specific sequence motifs with its C-terminal zinc-finger domain (Ségurel et al. 2011), the histone methyltransferase PRDM9 trimethylates H3K4 and H3K36 (Powers et al. 2016), thereby creating an open chromatin environment permissive to the formation of DNA double-strand breaks (Neale and Keeney 2006). Programed meiotic double-strand breaks are subsequently repaired using the homologous chromosome as a template (San Filippo et al. 2008), leading to either a reciprocal exchange of large segments of genetic material between the homologs (crossover; CO) or, more commonly, a nonreciprocal transfer of a short segment from a donor homolog (noncrossover; NCO) (Sun et al. 1989; and see the reviews of Wang et al. 2015; Lorenz and Mpaulo 2022).

Although a common determinant of recombination landscapes in primates, the location of PRDM9-mediated hotspots appears generally nonconserved between species (e.g. Auton et al. 2012; Stevison et al. 2016; and see Baker et al. 2017), as the rapid evolution of the PRDM9 zinc-finger domain alters the recognition of, and binding specificity to, the sequence motif (Oliver et al. 2009; Myers et al. 2010; Hinch et al. 2011; Baudat et al. 2013; Baker et al. 2017). In many organisms, there also exist sex-specific differences with regards to both the positioning and usage of recombination hotspots as well as the overall rate of recombination; for example, in humans, females generally exhibit higher rates of COs and lower rates of NCOs than males (though NCO tracts tend to be longer), whereas males display a more prominent elevation of recombination rates toward the telomeric ends of the chromosomes compared to the more uniformly distributed rates observed in females (Kong et al. 2002, 2010; Coop et al. 2008; Halldorsson et al. 2016, 2019; Palsson et al. 2025; and see Sardell and Kirkpatrick 2020).

Knowledge of the distribution and frequency of recombination is vitally important in many studies of molecular evolution and population genetics, including, for instance, in the inference of population history, the detection of genomic targets of natural selection, as well as genome-wide association and linkage studies (Johri et al. 2022). Consequently, species-specific recombination landscapes have been inferred in a variety of primates of evolutionary and biomedical interest over the past decades, ranging from the great apes (e.g. Kong et al. 2002, 2010; Auton et al. 2012; Stevison et al. 2016; Bhérer et al. 2017; Halldorsson et al. 2019), to baboons (Wall et al. 2022), rhesus macaques (Xue et al. 2016, 2020; Versoza et al. 2024; Terbot et al. 2025b; Spatola et al. 2026), vervet monkeys (Pfeifer 2020), marmosets (Soni et al. 2025b), and aye-ayes (Soni et al. 2025c; Terbot et al. 2025a; Versoza et al. 2025; and see the review of Soni et al. 2025a). Notably though, much of this previous work indirectly inferred sex-averaged recombination rates at the population-level from patterns of linkage disequilibrium (LD) along the genome, focusing by and large on the outcome of CO events that reshuffle haplotypes. Conversely, despite occurring at much higher frequencies in the genomes of many organisms (Jeffreys and May 2004; Baudat and de Massy 2007; Cole et al. 2010; Comeron et al. 2012; Li et al. 2019; Palsson et al. 2025), NCO events remain relatively understudied, despite their importance to genome evolution, leaving our picture of recombination landscapes incomplete.

To address this gap in our knowledge, and to circumvent (potentially problematic) simplifying assumptions regarding the demographic history, effective population size, and mutation rate necessary for the application of LD-based approaches, a limited number of studies have recently begun to directly investigate CO and NCO events based on whole genome data from pedigreed individuals or from single-molecule sequences of individual sperm (or testis) samples (Coop et al. 2008; Williams et al. 2015; Halldorsson et al. 2016; Wall et al. 2022; Schweiger et al. 2024; Versoza et al. 2024, 2025; Palsson et al. 2025; Porsborg et al. 2025). However, in contrast to CO events which are relatively straightforward to identify, the detection of NCO events remains challenging (see the discussion in Li et al. 2019). Specifically, NCO detection is complicated by their short tract size (e.g. spanning ~50 to 1,000 bp in humans, with recent empirical estimates suggesting that the majority of NCOs are likely associated with PRDM9-mediated recombination and exhibit a mean conversion tract length of ~40 to 100 bp); a minor proportion, likely the result of a distinct process independent of PRDM9, exhibits longer mean conversion tract lengths (Jeffreys and May 2004; Odenthal-Hesse et al. 2014; Williams et al. 2015; Halldorsson et al. 2016; Hardarson et al. 2023; Schweiger et al. 2024; Palsson et al. 2025; Porsborg et al. 2025). Recent statistical inference of the underlying length distribution estimated an even lower overall mean length of ~20 bp (Masaki and Browning 2025). Importantly, given the necessity of a heterozygous marker intersecting with the affected segment of genetic material, one would further anticipate

that a greater proportion of events will be rendered undetectable as species-level heterozygosity is reduced (Charmouh et al. 2025). For levels of heterozygosity commonly observed in many primate genomes for example, NCO tracts frequently include only a single phase-informative marker (as is the case in >90% of NCOs observed in humans; Schweiger et al. 2024), thus care must be taken to reliably distinguish between genuine NCO events and sequencing/genotyping errors. Complicating detection even further are complex NCO events containing both converted and nonconverted markers (Webb et al. 2008). Despite these challenges, pedigree-based approaches remain quintessential in improving our understanding of sex-specific CO and NCO events. Yet, aside from humans and the handful of nonhuman primates in which these approaches have been applied (Williams et al. 2015; Halldorsson et al. 2016, 2019; Wall et al. 2022; Schweiger et al. 2024; Versoza et al. 2024; Palsson et al. 2025; Porsborg et al. 2025), detailed knowledge of the rates and patterns of recombination remains lacking in many species, in part due to limited sample availability.

In order to better illuminate the nature of these landscapes across the primate clade, we here consider the coppery titi monkey (*Plecturocebus cupreus*), a socially monogamous species characterized by small pair-bonded family groups native to the Amazon forests of Brazil and Peru (Kinzey 1997). Although fewer than 10% of mammals display social monogamy and pair-bonding in the wild (Kleiman 1977; Lukas and Clutton-Brock 2013), the prevalence of these traits in humans (Gavrilets 2012) and their importance to healthy ageing (House et al. 1988) has prompted the development of coppery titi monkeys as an important model system for the study of social behavior (e.g. Bales et al. 2007, 2017, 2021). To facilitate this research, a colony of coppery titi monkeys was established at the California National Primate Research Center (CNPRC) in the 1970s (Lorenz and Mason 1971). Yet, genome-wide association studies aimed at identifying genetic variants underlying these phenotypes of interest are currently hampered by a lack of both population genomic data and knowledge of the species-specific recombination landscape. Taking advantage of the recently released chromosome-level genome assembly (Pfeifer et al. 2024), together with high-coverage genomic data from 17 individuals belonging to three multi-sibling families, we here provide the first recombination rate estimates for the species and characterize the sex-specific spatial distribution of CO and NCO events along the genome. In addition to providing novel insights into the rates and patterns of recombination, the resulting genetic map will thus also serve as a valuable resource for future studies in this important behavioral model system.

Results and Discussion

To gain insights into the sex-specific landscapes of CO and NCO recombination in coppery titi monkeys, 9.3 million autosomal variants were called from high-coverage (~50×) genomic data of 17 individuals belonging to three multi-sibling families housed at the CNPRC (Fig. S1; and see Tables S1 and S2 for sample information and details of the variant dataset, respectively). Of these, an average of 4.2 million variants per family were informative with regards to the parent-of-origin of the haplotypes inherited by the offspring (Table S3; and see Table S4 and Figs. S2 to S4 for the density and distribution of the phase-informative markers across chromosomes in each family, respectively) and could thus be used to detect COs, consisting of a single switch in haplotype phase, and NCOs, consisting of short segments with two switches in haplotype phase in close proximity to one another (see "Materials and Methods" for more information).

Sex-specific Landscape of CO Recombination in Coppery Titi Monkeys

In the 22 meioses of the three multi-sibling coppery titi monkey families (Fig. S1), 579 putative autosomal CO events were detected. Out of these events, 40 were removed during manual curation as they formed tight clusters (≥3 COs within 10 Mb) within single meioses (Table S5)—an observation more likely to be a technical artifact resulting from local assembly errors than biologically genuine, as CO interference reduces the likelihood of several COs in close proximity on the same chromosome (Muller 1916; and see the review of Otto and Payseur 2019). As an expected result of such CO interference, of the remaining 539 COs, CO events occurring in the same meiosis were more distant than expected based on the distribution of COs in different meioses (Fig. S5a; and see Fig. S5b for a comparison between individuals).

The 265 maternally inherited and 274 paternally inherited COs could be resolved to intervals (i.e. regions in which a CO occurred) with a median resolution of 8.1 kb and 10.9 kb, respectively (Fig. S6). The genome-wide distribution of these COs is depicted in Fig. 1a (genomic locations are provided in Table S6; and see Figs. S7 to S28 for the haplotype blocks observed on each chromosome in each meiosis). At the broad-scale, a pronounced enrichment of COs near telomeres was observed in males (Fig. 1b), similar to other mammals (Lenormand and Dutheil 2005; Sardell and Kirkpatrick 2020). At the fine-scale, COs were highly localized in both intergenic and intronic regions (Fig. 2a) as

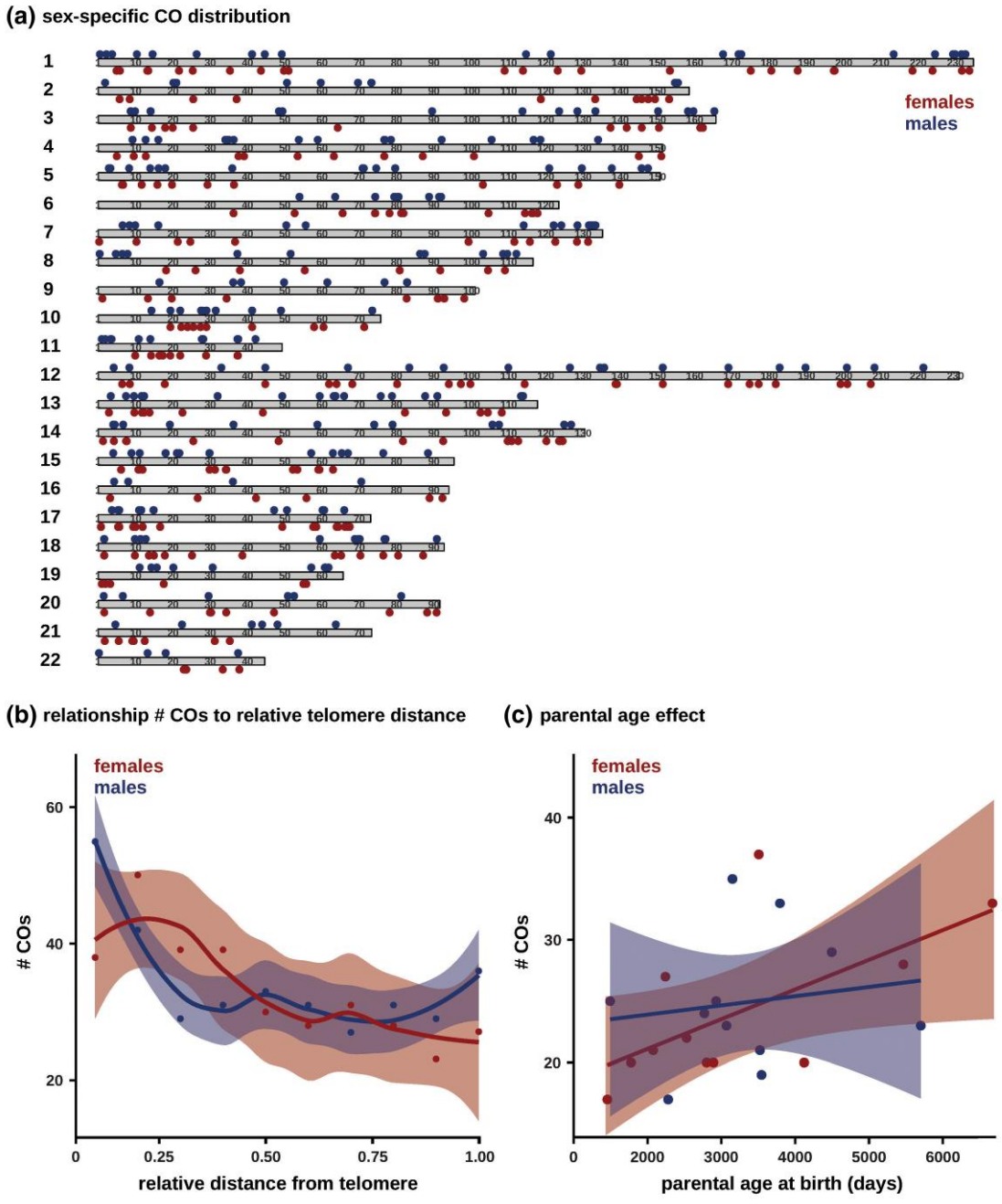

Fig. 1. CO recombination in coppery titi monkeys. a) Sex-specific CO distribution per autosome (chromosomes 1 to 22), with maternally inherited COs shown in red and paternally inherited COs shown in blue. b) Relationship between the sex-specific number of CO events and relative distance to the nearest telomere. c) Relationship between the sex-specific number of CO events and parental age at birth.

expected for PRDM9-mediated recombination (Coop et al. 2008); however, males and females displayed significant differences with regards to their overall genomic distribution of CO events ($\chi^2 = 7602.49$, df = 4, *P*-value < 0.0001) driven by an enrichment of COs in intergenic regions in females and in gene-associated regions (downstream, exonic, intronic, and upstream) in males. Providing further evidence of a functional PRDM9, COs were harbored within CpG islands no more frequently than expected by chance (Fig. S29) and COs were depleted around genes (Fig. S30), as expected given that PRDM9 tends to prevent meiotic recombination in close proximity to transcription start sites (Myers et al. 2005; Coop et al. 2008).

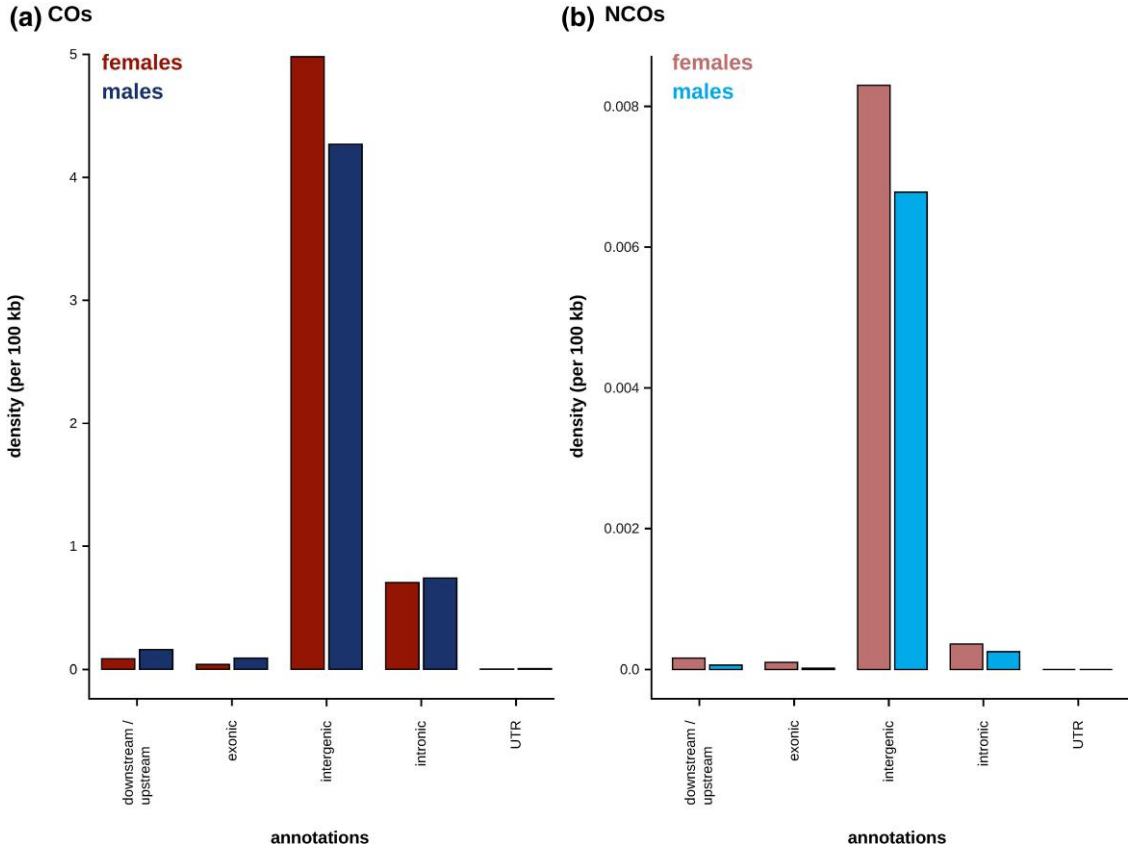

Fig. 2. CO and NCO recombination in coppery titi monkeys by genomic region. Density of sex-specific a) COs with a resolution of <10 kb and b) NCOs with a conversion tract length of <10 kb by genomic region.

On average, 23 COs were observed per meiosis (Table S7), with the average number of COs per chromosome significantly correlated with autosomal length (r = 0.78; P-value = 1.88 × 10^{-5}; Fig. S31). Most primates studied to date exhibit higher recombination rates in females (see the review of Sardell and Kirkpatrick 2020); however, a similar number of COs were observed in both sexes in the three coppery titi monkey families, with an average of 1.10 COs and 1.13 COs per autosome per meiosis in the 11 maternal and 11 paternal meioses, respectively (two-tailed binomial test: P-value = 0.698; Table S7), consistent with one obligatory CO per chromosome arm (Pardo-Manuel de Villena and Sapienza 2001). Due to these similarities in genome-wide CO rates (on average 1.00 cM/Mb and 1.04 cM/Mb in females and males, respectively), sex-specific autosomal genetic maps were also alike (2,409 cM vs. 2,491 cM; Table 1; and see Fig. S32 for the cumulative genetic distance per chromosome in males and females). The estimated sex-averaged autosomal genetic map in coppery titi monkeys (2,450 cM) was observed to be about 30% shorter than the sex-averaged autosomal genetic map in humans (Kong et al. 2002), despite the same karyotype ($2n$ = 46; Dumas et al. 2005). Although the map length reported here is likely an underestimate due to the small sample size of this study (relative to existing studies in humans), it is noteworthy that similar differences from humans have been observed in other nonhuman primates (Rogers et al. 2000, 2006; Cox et al. 2006; Jasinska et al. 2007; Wall et al. 2022; Versoza et al. 2024, 2025; and see the review of Coop and Przeworski 2007).

Notably, the number of CO events in females was significantly positively correlated with maternal age (r = 0.62; P-value = 0.043; Fig. 1c), with an estimated 0.7 additional COs per year. A maternal age effect on recombination has also previously been observed in humans (Kong et al. 2004; Coop et al. 2008; Martin et al. 2015; Halldorsson et al. 2019; though see Hussin et al. 2011 and Porubsky et al. 2025) and has been suggested to be potentially driven by selection as a larger number of COs along homologous chromosomes may increase the stability of the bivalent (Robinson et al. 1998) and thus serve to counteract maternal age-related nondisjunction driven by the long period of meiotic arrest of oocytes which frequently leads to aneuploidy and

Table 1 Sex-specific genetic linkage maps (male/female)

Chromosome	Length (Mb)	No. of CO events	cM	cM/Mb
1	235.10	23/24	209.1/218.2	0.89/0.93
2	158.74	13/11	118.2/100.0	0.74/0.63
3	165.94	15/12	136.4/136.4	0.82/0.66
4	151.62	16/15	145.5/136.4	0.96/0.90
5	150.99	16/11	145.5/100.0	0.96/0.66
6	123.74	9/14	81.8/127.3	0.66/1.03
7	135.51	14/11	127.3/100.0	0.94/0.74
8	116.83	12/8	109.1/72.7	0.93/0.62
9	101.23	9/10	81.8/90.9	0.81/0.90
10	75.88	13/10	118.2/90.9	1.56/1.20
11	49.37	13/10	118.2/90.9	2.39/1.84
12	231.18	19/24	172.7/218.2	0.75/0.94
13	118.03	20/12	181.8/109.1	1.54/0.92
14	130.78	13/15	118.2/136.4	0.90/1.04
15	95.53	16/13	145.5/118.2	1.52/1.24
16	94.17	4/6	36.4/54.5	0.39/0.58
17	73.18	12/17	109.1/154.5	1.49/2.11
18	92.88	12/15	109.1/136.4	1.17/1.47
19	65.77	9/7	81.8/63.6	1.24/0.97
20	91.75	6/9	54.5/81.8	0.59/0.89
21	73.43	6/7	54.5/63.6	0.74/0.87
22	44.72	4/4	36.4/36.4	0.81/0.81
Autosomal	2,576.39	274/265	2,491/2,409	1.04/1.00
(Sex-averaged)		(269.5)	(2,450)	(1.02)

fetal loss (see the review of Hassold et al. 2000; Carioscia et al. 2026). In further concordance with humans, no statistically significant paternal age effect was observed for coppery titi monkeys ($r = 0.15$; P-value = 0.657).

Identification of a Putative PRDM9 Sequence and Binding Motifs

In primates, as in many other sexually reproducing organisms, recombination hotspots are generally localized by the histone methyltransferase PRDM9 (Baudat et al. 2010; Myers et al. 2010; Parvanov et al. 2010). Although genes in the coppery titi monkey genome were previously characterized (Pfeifer et al. 2024), no annotation was available for PRDM9. As the highly repetitive nature and rapid evolution of PRDM9 makes the gene prone to mis-assembly, previously generated long-read data (Pfeifer et al. 2024) was thus used together with information from the human PRDM9 sequence to de novo assemble a putative PRDM9 sequence in coppery titi monkeys. A BLASTX (Altschul et al. 1990) search provided support for a high sequence similarity of the re-assembled contig with PRDM9 sequences of other primates, including the central SSXRD and PR/SET domains as well as three C-terminal zinc fingers (Fig. S33); however, no N-terminal KRAB domain could be identified. The KRAB domain is an integral component of PRDM9 (Hohenauer and Moore 2012), necessary for double-strand repair and synapsis during meiosis, with previous research demonstrating that a domain truncation leads to a loss of PRDM9 function (Imai et al. 2017). Although certain strepsirrhines appear to be lacking the KRAB domain (Baker et al. 2017), given that the observed CO patterns are in general agreement with PRDM9-mediated recombination, the contig thus likely represents a partial or truncated PRDM9 ortholog, with the lack of a KRAB domain reflecting either an incomplete assembly or difficulties in the domain recognition or gene prediction due to its rapid evolution (Imbeault et al. 2017). Additional support for a functional PRDM9 was provided by gene expression observed in a previously collected testis sample, but not in the samples of heart and adrenal glands (Table S8).

Analyses of high-resolution CO breakpoints identified a putative 15-mer PRDM9 binding motif, CCTGCCTCAG CCTCC, which shows considerable similarities to the degenerate 13(−15)-mer motif of the common PRDM9 A allele in humans, (N)CCNCCNTNNCCNC(N) (Myers et al. 2008; Baudat et al. 2010; Pratto et al. 2014; Patel et al. 2016; Altemose et al. 2017), including the well-defined spacing of multiple CC dinucleotides and generally high GC-content (Fig. S34). Similar to humans, in which the degenerate 13-mer motif is predicted to recruit COs to ~40% of hotspots (Myers et al. 2008), the 15-mer motif identified in coppery titi monkeys is harbored within

43% of the CO breakpoint regions—a significant enrichment compared to the genomic background (Fisher's exact test, *P*-value = 1.10×10^{-35}).

Sex-specific Landscape of NCO Recombination in Coppery Titi Monkeys

A total of 287 putative autosomal NCO events were detected in the 22 meioses of the three coppery titi monkey families (Fig. S1). Out of these events, 103 (35.9%) were removed as they failed at least one of the stringent filter criteria applied to circumvent genotyping errors. Specifically, seven events were removed due to low-confidence read mappings (with five and two events based on read mappings with an average depth of coverage of ≤ 20 and an average mapping quality of ≤ 40 across individuals, respectively), four events were removed as they were located within 10 phase-informative markers from the end of a chromosome, 58 events were removed as they were harbored within regions characterized by frequent haplotype changes (with <10 markers showing a consistent haplotype phase on either side of the event), 29 events were removed because they coincided with another putative NCO in the surrounding 1-kb region, three events were removed due to a change of phase within the same region in another meiosis, and two events were removed because they overlapped with structural variation previously identified in the population (Versoza et al. 2026).

Of the final 184 NCOs (Table S9), the vast majority (163, or 88.6%) were supported by a single marker, thus resulting in minimal conversion tract lengths of 1 bp, in agreement with previous observations in humans (92.8%; Schweiger et al. 2024). Among the 21 NCOs supported by more than one marker, 17 exhibited a mean minimal NCO conversion tract length of 55 bp (range: 2 to 350 bp), similar to those previously observed in other primates (Wall et al. 2022; Versoza et al. 2024, 2025; Charmouh et al. 2025; Porsborg et al. 2025). The remaining four NCOs exhibited minimal conversion tract lengths >10 kb, with the two largest events being particularly poorly resolved. Previous research has demonstrated that such NCOs detected from short-read data frequently represent technical artifacts (Wall et al. 2022), thus the analyses presented here focused on the 180 NCO events with a tract length shorter than 10 kb.

The genome-wide distribution of the final 97 maternally inherited and 83 paternally inherited NCOs is depicted in Fig. 3a (genomic locations are provided in Table S9; and see Figs. S7 to S28 for the NCOs observed on each chromosome in each meiosis). Thereby, NCO events occurring in the same meiosis were similarly spaced apart than those occurring in different meioses (Fig. S35a; and see Fig. S35b for a comparison between individuals). In agreement with humans, where NCOs—like COs—are often concentrated at PRDM9-mediated hotspots (Williams et al. 2015; Halldorsson et al. 2016), the majority (52.8%) of short (10 kb) regions centered around NCOs contained the putative 15-mer PRDM9 binding motif. Analogous to COs, NCOs were localized in intergenic and, to a lesser extent, intronic regions (Fig. 2b) but with a more similar overall genomic distribution between the sexes ($\chi^2 = 6.8332$, df = 3, *P*-value = 0.077). Sex-specific differences exist, however, with regards to the minimal conversion tract lengths of extended events which, consistent with previous observations in humans (Palsson et al. 2025), were considerably longer in maternally inherited NCOs than in paternally inherited NCOs (72.8 bp vs. 30.7 bp; Table S9). Independent of sex, the overall distribution of minimal conversion tract lengths (Fig. 3b) mimics those observed in other species (e.g. Williams et al. 2015; Halldorsson et al. 2016; Wall et al. 2022; Versoza et al. 2024, 2025; Palsson et al. 2025). Notably though, in contrast to the GC-biased gene conversion observed in these species (see the review of Duret and Galtier 2009), no transmission bias toward strong alleles (C or G) was detected in the dataset (45.1%).

Per meiosis, between 0 and 16 NCOs were identified, with an average of 8.8 and 7.6 NCOs in females and males, respectively, resulting in a combined sex-averaged rate of 0.37 NCOs per autosome (Table S7). This estimate is considerably lower than the average number of NCOs observed in both humans (~2 to 3 NCOs per chromosome and meiosis; Palsson et al. 2025) and rhesus macaques (~1 NCO per chromosome and meiosis; Versoza et al. 2024) and likely represents an underestimate due to both the stringent filtering criteria applied and the status of the coppery titi monkey genome assembly compared to the near-complete telomere-to-telomere assemblies available for these biomedically-relevant species. For comparison, a recent study in aye-ayes, which relied on an assembly with a similar contiguity to that of coppery titi monkeys (930 contigs with a contig N50 of 80.4 Mb in aye-ayes [Versoza and Pfeifer 2024] vs. 2,013 contigs with a contig N50 of 17 Mb in coppery titi monkeys [Pfeifer et al. 2024]), observed only a slightly higher rate of NCOs (~0.7 NCOs per chromosome and meiosis; Versoza et al. 2025). Therefore, in order to estimate the power to detect NCO events present in this study, 2,000 NCO events were simulated based on the tract length distributions observed in humans (Palsson et al. 2025). In concordance with recent work demonstrating a low power to detect short conversion tracts (~2 to 4% in humans; Palsson et al. 2025), only 7.3% of short tracts were identifiable in coppery titi monkeys.

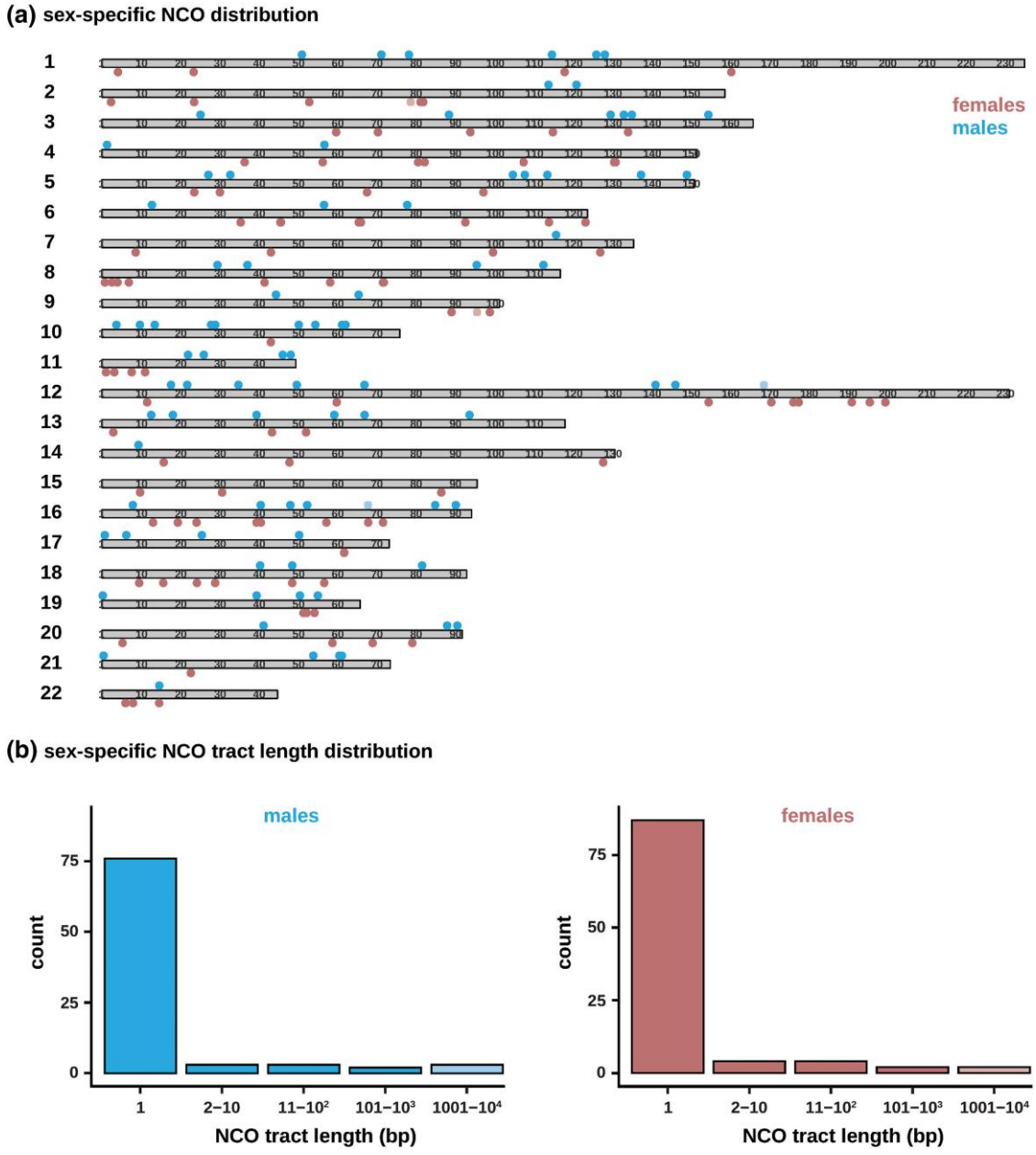

Fig. 3. NCO recombination in coppery titi monkeys. a) Sex-specific NCO distribution per autosome (chromosomes 1 to 22), with maternally inherited NCOs shown in red and paternally inherited NCOs shown in blue (NCO events > 10 kb are indicated by shading). b) Sex-specific minimal NCO conversion tract length distributions.

Power was considerably higher (90.1%) for extended conversion tracts due to the high marker density; nevertheless, as most NCO events tend to be short, it is expected that the genuine number of bases affected by NCOs will be much larger.

Taken together, in addition to providing the first insights into the sex-specific landscapes of CO and NCO recombination in coppery titi monkeys, the resources generated in this study will also enable future evolutionary studies, including those aiming to understand the selective pressures shaping the genome of this important socially monogamous, pair-bonded behavioral primate model.

Materials and Methods

Ethics Statement

This study was performed in compliance with all regulations regarding the care and use of captive primates, including the NIH Guidelines for the Care and Use of

Animals and the American Society of Primatologists' Guidelines for the Ethical Treatment of Nonhuman Primates. Procedures were approved by the UC-Davis Institutional Animal Care and Use Committee (protocol 22523).

Samples and Sequencing

Peripheral blood samples were collected from 17 coppery titi monkeys (*P. cupreus*) belonging to three multisibling families housed at the CNPRC (Fig. S1; and see Table S1 for sample information). Genomic DNA was extracted from whole blood samples using the PAXgene Blood DNA System or the QIAamp DNA Mini Kit (Qiagen, Hilden, Germany), the DNA concentration of each sample was measured using an Invitrogen Qubit Fluorometer (Thermo Fisher Scientific, Waltham, MA, US), and sample integrity and purity were assessed using Agarose Gel Electrophoresis. PCR-free libraries were prepared for all samples, checked with Qubit and real-time PCR for quantification and bioanalyzer for size distribution detection, and paired-end sequenced (2×150 bp) on an Illumina NovaSeq 6000 (Illumina, San Diego, CA, USA).

Whole Genome Alignment

Raw reads were preprocessed using fastp v.0.24.0 (Chen et al. 2018) which detects and trims both sequencing adapters in paired-end data (*–detect_adapter_for_pe*) and polyG tails common in Illumina NovaSeq data (default minimum length: 10 bp). Additionally, fastp automatically performs quality and length filtering, removing any reads that contain more than 40% of bases with a Phred quality score of <15, more than five bases without call information (Ns), or an overall length of less than 15 bp. Quality-controlled reads were aligned to the coppery titi monkey reference genome (GenBank accession number: GCA_040437455.1; Pfeifer et al. 2024) using the GPU-accelerated NVIDIA Parabricks v.4.4.0-1 implementation of the Burrows-Wheeler Aligner (Li 2013), marking shorter split hits as secondary (*-M* option). Depth of coverage for each sample is provided in Table S1.

Variant Discovery

Prior to calling variants, duplicates were marked using the NVIDIA Parabricks v.4.4.0-1 implementation of the Genome Analysis Toolkit (GATK; van der Auwera and O'Connor 2020) to eliminate spurious read coverage support (Pfeifer 2017). Given the lack of polymorphism data for the species, a first round of variant calling was performed on the high-quality, duplicate-marked mappings (*–minimum-mapping-quality 40*) of each sample, using the GATK *HaplotypeCaller* without PCR correction (*-pcr-indel-model NONE*), following the developers' recommendations. Resulting genomic variant call files were then merged (*CombineGVCF*) to allow for joint genotyping across samples (*GenotypeGVCF*). In order to create a high-confidence dataset, annotations informative for bootstrapping were plotted for single-nucleotide polymorphisms (SNPs) to determine appropriate filtering thresholds that control the transition-transversion ratio (for details, see Auton et al. 2012); subsequently any SNPs supported by less than half, or more than twice, a sample's mean autosomal read depth (*DP*), exhibiting a genotype quality (*GQ*) of <60, a quality-by-depth (*QD*) of <10, a mapping quality rank sum test (*MQRankSum*) score of <−12.5, or a read position rank sum (*ReadPosRankSum*) score of <−8.0, or showing any signs of strand bias as determined by a Fisher's exact test ($FS > 5$) or symmetric odds ratio ($SOR > 1.5$), were removed from the dataset using BCFtools *filter* v.1.14 (Danecek et al. 2021). GATK's machine-learning-based base quality score recalibration procedure (*BaseRecalibrator* and *ApplyBQSR*) was then used to model systematic errors present in the sequencing data and to adjust the base quality scores of the original, duplicate-marked mappings to more accurately reflect the probability of a base call being incorrect. Subsequently, a second round of variant calling was performed on the recalibrated mappings as described above. To further improve accuracy, biallelic SNPs that contained genotype information for all individuals in the pedigrees were re-genotyped using Graphtyper v.2.7.2 (Eggertsson et al. 2017), a graph-based genotyping approach shown to improve variant detection, particularly in complex genomic regions. Due to the lower read depth on, and different ploidies of, the sex chromosomes (X and Y), the re-genotyped dataset was limited to autosomal sites that passed all built-in sample and record level filters.

As the detection of CO and NCO events is sensitive to genotyping errors, the dataset was restricted to regions of the reference genome in which the 150bp-long sequencing reads could be confidently mapped. To this end, an accessibility mask with a stringency of 1 was generated using the *SNPable* workflow (https://lh3lh3.users.sourceforge.net/snpable.shtml), and any regions not deemed confidently mappable were excluded from downstream analyses. Additionally, the variant dataset was limited to sites consistent with the patterns of Mendelian inheritance located farther than 10 bp from the nearest insertion/deletion, with a depth of coverage of at least half, but no more than twice, the average autosomal coverage for each individual. Lastly, to ensure that heterozygous calls were of high quality, genotypes exhibiting an allelic imbalance (*P*-value of >0.01 in a two-sided exact binomial test) were filtered out

following Prentout et al. 2025. Details of the variant dataset are provided in Table S2.

Detection of Recombination Events

Recombination events were detected by tracing gamete transmission across the multiple-offspring families (including a total of 11 maternal meioses and 11 paternal meioses; Fig. S1). To this end, phase-informative markers—that is, sites at which only one of the parents exhibits a heterozygous genotype—observed in a family were first used to distinguish between maternally and paternally inherited haplotypes in each offspring (see Table S3 for the number, Table S4 for the per-chromosome density, and Figs. S2 to S4 for the distribution of phase-informative markers per family). This assignment allowed for the subsequent detection of recombination events through the comparison of phase-informative markers inherited by each sibling of a multi-offspring family in order to identify switches in the parental haplotype phase (Coop et al. 2008; and see Fig. S20 in Versoza et al. 2025 for a schematic representation of this approach). Following the methodology outlined in Prentout et al. 2025, recombination events were separated into COs (a single switch in haplotype phase) and NCOs (two phase changes occurring in close proximity and surrounded by the same parental haplotype). To guard against genotyping errors, putative CO events located within 10 phase-informative markers in an individual meiosis were grouped, keeping only COs with a single switch in haplotype, and CO events within 10 phase-informative markers from the chromosomal ends were removed. Subsequently, all putative CO events were manually inspected and those forming tight clusters (defined here as ≥ 3 COs within 10 Mb, as per Wall et al. 2022) were removed (Table S5). In a similar vein, as putative NCO events tend to be short, frequently involving only a single phase-informative marker, such markers were required to be supported by high-confidence read mappings (defined here as read mappings with an average depth of coverage of >20 and an average mapping quality of >40 across individuals) and located more than 10 phase-informative markers away from the chromosomal ends; additionally, NCO tracts were required to be enclosed by $\geq$10 markers with consistent haplotype phase on either side (as per Prentout et al. 2025). Moreover, putative NCO events with a switch in haplotype phase in the same genomic location in any other meiosis, as well as those coinciding with another NCO in the surrounding 1-kb region, were excluded to avoid spurious events caused by genome assembly errors. Finally, putative NCO events overlapping structural variants known to segregate in the population (Versoza et al. 2026) were excluded from downstream analyses. A summary of the final recombination events is provided in Table S7, with details of the detected CO and NCO events given in Tables S6 and S9, respectively.

Annotation of Recombination Events

CO events with a high resolution (<10 kb) and NCO events with a short tract length (<10 kb) were annotated using ANNOVAR v.2020-06-08 (Wang et al. 2010) to determine overlaps with genomic features. In addition, overlaps with CpG islands were categorized based on the annotations obtained from the reference genome (Pfeifer et al. 2024) via the *newcpgreport* function implemented in the EMBOSS suite (Rice et al. 2020; Madeira et al. 2022).

Identification of a Putative PRDM9 Sequence and Binding Motifs

To identify a putative PRDM9 sequence in coppery titi monkeys, Liftoff v.1.6.3 (Shumate and Salzberg 2021) was used to project the human PRDM9 sequence from UniProt (entry: Q9NQV7; UniProt Consortium 2025) onto the coppery titi monkey assembly. As the highly repetitive nature and rapid evolution of PRDM9 makes the gene prone to mis-assembly, previously generated long-read data was aligned against the current reference genome assembly (Pfeifer et al. 2024) with minimap2 v.2.24 (using the recommended Oxford Nanopore preset '*-ax* map-ont'; Li 2018), the 2-Mb region encompassing the putative PRDM9 sequence identified by Liftoff was extracted using SAMtools v.1.16 (Danecek et al. 2021), and subsequently re-assembled using Flye v.2.9.1 (Kolmogorov et al. 2019). The resulting contig was then mapped back to the human PRDM9 sequence using GeneWise v.2.4.1 (Birney et al. 2004) to predict gene structure. To ensure that the extracted sequence was of high quality, it was translated into amino acids using the ExPASy platform (Gasteiger et al. 2003) and manually inspected using InterPro (Blum et al. 2025). Additionally, a BLASTX (Altschul et al. 1990) search was performed against the nonredundant protein sequences (nr) database in primates (taxid: 9443) to confirm PRDM9 identity and to manually inspect for both the presence and completeness of the KRAB, SSXRD, PR/SET, and zinc-finger domains based on identified conserved domains.

To help determine whether the identified PRDM9 was likely functional, patterns of gene expression of a previously collected testis sample were compared to those of heart and adrenal glands (Pfeifer et al. 2024), with the latter two serving as negative controls as PRDM9 is expressed during meiosis. To this end, RNAseq data from these tissues were first trimmed

using Trimmomatic v.0.39 (Bolger et al. 2014) in paired-end mode (with the '*LEADING*: 3', '*TRAILING*: 3', and '*MINLEN*: 36' flags enabled) before mapping the reads to the coppery titi monkey reference genome (Pfeifer et al. 2024) containing the putative PRDM9 contig using STAR v.2.7 (Dobin et al. 2013). Presence or absence of gene expression was assessed based on properly paired reads that mapped uniquely to the putative PRDM9 contig (Table S8).

High-resolution CO events were used to identify putative PRDM9 binding motifs. In brief, following the approach described in Wijnker et al. (2013), each high-resolution CO event was expanded by 500 bp on either side to capture the entire interval likely involved in the double-strand break formation and repair. Based on these breakpoint intervals, a de novo motif discovery was then performed using MEME v.5.5.7 (Bailey and Elkan 1994) under the ZOOPS model with a significance threshold of 1e-05, assuming that sequence motifs exhibit a length between 5 and 15 nucleotides. To mitigate sequence composition bias during this search, a background model was generated from randomly chosen genomic regions that matched the breakpoint intervals in overall size and GC-content. Given the high repetitiveness of PRDM9 motifs in humans and other primates (e.g. Altemose et al. 2017), a permutation test was carried out using MOODS v.1.9.4.1 (Korhonen et al. 2009), comparing the frequencies of the discovered motif between the breakpoint intervals and 1,000 randomly sampled nonbreakpoint intervals (*P*-value cutoff for matches: 0.05). The statistical significance of the observed enrichment in breakpoint intervals was evaluated using a Fisher's exact test in R v.4.2.2 (R Core Team 2024).

Estimating the Power to Detect NCO Events

In order to estimate the power to detect NCO events present in the population genomic data analyzed in this study, 2,000 NCO events were simulated based on the tract length distributions observed in humans (Palsson et al. 2025). Specifically, to generate length distributions for NCO tracts that mimic empirical data, tract lengths were simulated following a normal distribution, with either a mean length of 102 bp and 123 bp for maternal and paternal short tracts, respectively, or a mean length of 9.1 kb and 7.2 kb for maternal and paternal long tracts, respectively (Palsson et al. 2025). For each tract category, the bounds were specified to match those observed in humans (maternal short tracts: 71 to 125 bp, paternal short tracts: 94 to 135 bp, maternal long tracts: 6.8 to 10.8 kb, paternal long tracts: 1.8 to 11.8 kb; Palsson et al. 2025). Using these parameters, 500 lengths were randomly drawn for each tract category from a normal distribution in R v.4.2.2 (R Core Team 2024), for a total of 2,000 lengths and, for each sampled length, a genomic region was randomly selected using BEDTools *random* v.2.3.0 (Quinlan and Hall 2010). Using these simulated regions, power was then estimated by dividing the number of NCO events that included at least one phase-informative marker (and were hence detectable) by the number of simulated events (i.e. detectable and nondetectable) (see "Detection of recombination events" for methodological details of the NCO detection procedure).

Supplementary Material

Supplementary material is available at Genome Biology and Evolution online.

Acknowledgments

DNA extraction, library preparation, and Illumina sequencing were conducted at the DNA Technologies and Expression Analysis Core at the UC Davis Genome Center (supported by NIH Shared Instrumentation Grant 1S10OD010786-01) and Novogene (Sacramento, CA, USA). Computations were performed on the Sol supercomputer at Arizona State University (Jennewein et al. 2023).

Funding

This work was supported by the National Institute of General Medical Sciences of the National Institutes of Health under Award Number R35GM151008 to S.P.P. and the California National Primate Research Center Pilot Program (NIH P51OD011107). C.J.V. was supported by the National Science Foundation CAREER Award DEB-2045343 to S.P.P. K.L.B. was supported by the Eunice Kennedy Shriver National Institute of Child Health and Human Development and the National Institute of Mental Health of the National Institutes of Health under Award Numbers R01HD092055 and MH125411, and by the Good Nature Institute. J.D.J. was supported by National Institutes of Health Award Number R35GM139383. The content is solely the responsibility of the authors and does not necessarily represent the official views of the funders.

Conflict of Interest

None declared.

Data Availability

Sequence data are available at NCBI BioProjects PRJNA1356510 and PRJNA1356860.

Literature Cited

Altemose N, et al. A map of human PRDM9 binding provides evidence for novel behaviors of PRDM9 and other zinc-finger proteins in meiosis. Elife. 2017:6:e28383. https://doi.org/10.7554/eLife.28383.

Altschul SF, Gish W, Miller W, Myers EW, Lipman DJ. Basic local alignment search tool. J Mol Biol. 1990:215:403–410. https://doi.org/10.1016/S0022-2836(05)80360-2.

Auton A, et al. A fine-scale chimpanzee genetic map from population sequencing. Science. 2012:336:193–198. https://doi.org/10.1126/science.1216872.

Bailey TL, Elkan C. Fitting a mixture model by expectation maximization to discover motifs in biopolymers. Proc Int Conf Intell Syst Mol Biol. 1994:2:28–36.

Baker Z, et al. Repeated losses of PRDM9-directed recombination despite the conservation of PRDM9 across vertebrates. Elife. 2017:6:e24133. https://doi.org/10.7554/eLife.24133.

Bales KL, et al. Titi monkeys as a novel non-human primate model for the neurobiology of pair bonding. Yale J Biol Med. 2017:90:373–387.

Bales KL, et al. What is a pair bond? Horm Behav. 2021:136:105062. https://doi.org/10.1016/j.yhbeh.2021.105062.

Bales KL, Mason WA, Catana C, Cherry SR, Mendoza SP. Neural correlates of pair-bonding in a monogamous primate. Brain Res. 2007:1184:245–253. https://doi.org/10.1016/j.brainres.2007.09.087.

Baudat F, et al. PRDM9 is a major determinant of meiotic recombination hotspots in humans and mice. Science. 2010:327:836–840. https://doi.org/10.1126/science.1183439.

Baudat F, de Massy B. Regulating double-stranded DNA break repair towards crossover or non-crossover during mammalian meiosis. Chromosome Res. 2007:15:565–577. https://doi.org/10.1007/s10577-007-1140-3.

Baudat F, Imai Y, de Massy B. Meiotic recombination in mammals: localization and regulation. Nat Rev Genet. 2013:14:794–806. https://doi.org/10.1038/nrg3573.

Bhérer C, Campbell CL, Auton A. Refined genetic maps reveal sexual dimorphism in human meiotic recombination at multiple scales. Nat Commun. 2017:8:14994. https://doi.org/10.1038/ncomms14994.

Birney E, Clamp M, Durbin R. GeneWise and genomewise. Genome Res. 2004:14:988–995. https://doi.org/10.1101/gr.1865504.

Blum M, et al. InterPro: the protein sequence classification resource in 2025. Nucleic Acids Res. 2025:53:D444–D456. https://doi.org/10.1093/nar/gkae1082.

Bolger AM, Lohse M, Usadel B. Trimmomatic: a flexible trimmer for Illumina sequence data. Bioinformatics. 2014:30:2114–2120. https://doi.org/10.1093/bioinformatics/btu170.

Carioscia SA, et al. Common variation in meiosis genes shapes human recombination and aneuploidy. Nature. 2026:651:146–153. https://doi.org/10.1038/s41586-025-09964-2.

Charmouh AP, et al. Estimating gene conversion tract length and rate from PacBio HiFi data. Mol Biol Evol. 2025:42:msaf019. https://doi.org/10.1093/molbev/msaf019.

Chen S, Zhou Y, Chen Y, Gu J. Fastp: an ultra-fast all-in-one FASTQ preprocessor. Bioinformatics. 2018:34:i884–i890. https://doi.org/10.1093/bioinformatics/bty560.

Cole F, Keeney S, Jasin M. Comprehensive, fine-scale dissection of homologous recombination outcomes at a hot spot in mouse meiosis. Mol Cell. 2010:39:700–710. https://doi.org/10.1016/j.molcel.2010.08.017.

Comeron JM, Ratnappan R, Bailin S. The many landscapes of recombination in *Drosophila melanogaster*. PLoS Genet. 2012:8:e1002905. https://doi.org/10.1371/journal.pgen.1002905.

Coop G, Przeworski M. An evolutionary view of human recombination. Nat Rev Genet. 2007:8:23–34. https://doi.org/10.1038/nrg1947.

Coop G, Wen X, Ober C, Pritchard JK, Przeworski M. High-resolution mapping of crossovers reveals extensive variation in fine-scale recombination patterns among humans. Science. 2008:319:1395–1398. https://doi.org/10.1126/science.1151851.

Cox LA, Mahaney MC, Vandeberg JL, Rogers J. A second-generation genetic linkage map of the baboon (*Papio hamadryas*) genome. Genomics. 2006:88:274–281. https://doi.org/10.1016/j.ygeno.2006.03.020.

Danecek P, et al. Twelve years of SAMtools and BCFtools. GigaScience. 2021:10:giab008. https://doi.org/10.1093/gigascience/giab008.

Dobin A, et al. STAR: ultrafast universal RNA-Seq aligner. Bioinformatics. 2013:29:15–21. https://doi.org/10.1093/bioinformatics/bts635.

Dumas F, Bigoni F, Stone G, Sineo L, Stanyon R. Mapping genomic rearrangements in titi monkeys by chromosome flow sorting and multidirectional in-situ hybridization. Chromosome Res. 2005:13:85–96. https://doi.org/10.1007/s10577-005-7063-y.

Duret L, Galtier N. Biased gene conversion and the evolution of mammalian genomic landscapes. Annu Rev Genomics Hum Genet. 2009:10:285–311. https://doi.org/10.1146/annurev-genom-082908-150001.

Eggertsson HP, et al. Graphtyper enables population-scale genotyping using pangenome graphs. Nat Genet. 2017:49:1654–1660. https://doi.org/10.1038/ng.3964.

Gasteiger E, et al. ExPASy: the proteomics server for in-depth protein knowledge and analysis. Nucleic Acids Res. 2003:31:3784–3788. https://doi.org/10.1093/nar/gkg563.

Gavrilets S. Human origins and the transition from promiscuity to pair-bonding. Proc Natl Acad Sci U S A. 2012:109:9923–9928. https://doi.org/10.1073/pnas.1200717109.

Halldorsson BV, et al. The rate of meiotic gene conversion varies by sex and age. Nat Genet. 2016:48:1377–1384. https://doi.org/10.1038/ng.3669.

Halldorsson BV, et al. Characterizing mutagenic effects of recombination through a sequence-level genetic map. Science. 2019:363:eaau1043. https://doi.org/10.1126/science.aau1043.

Hardarson MT, Palsson G, Halldorsson BV. NCOurd: modelling length distributions of NCO events and gene conversion tracts. Bioinformatics. 2023:39:btad485. https://doi.org/10.1093/bioinformatics/btad485.

Hassold T, Sherman S, Hunt P. Counting cross-overs: characterizing meiotic recombination in mammals. Hum Mol Genet. 2000:9:2409–2419. https://doi.org/10.1093/hmg/9.16.2409.

Hinch AG, et al. The landscape of recombination in African Americans. Nature. 2011:476:170–175. https://doi.org/10.1038/nature10336.

Hohenauer T, Moore AW. The PRDM family: expanding roles in stem cells and development. Development. 2012:139:2267–2282. https://doi.org/10.1242/dev.070110.

House JS, Landis KR, Umberson D. Social relationships and health. Science. 1988:241:540–545. https://doi.org/10.1126/science.3399889.

Hussin J, Roy-Gagnon MH, Gendron R, Andelfinger G, Awadalla P. Age-dependent recombination rates in human pedigrees. PLoS Genet. 2011:7:e1002251. https://doi.org/10.1371/journal.pgen.1002251.

Imai Y, et al. The PRDM9 KRAB domain is required for meiosis and involved in protein interactions. Chromosoma. 2017:126:681–695. https://doi.org/10.1007/s00412-017-0631-z.

Imbeault M, Helleboid PY, Trono D. KRAB zinc-finger proteins contribute to the evolution of gene regulatory networks. Nature. 2017:543:550–554. https://doi.org/10.1038/nature21683.
Jasinska AJ, et al. A genetic linkage map of the vervet monkey (*Chlorocebus aethiops sabaeus*). Mamm Genome. 2007:18: 347–360. https://doi.org/10.1007/s00335-007-9026-4.
Jeffreys AJ, May CA. Intense and highly localized gene conversion activity in human meiotic crossover hot spots. Nat Genet. 2004:36:151–156. https://doi.org/10.1038/ng1287.
Jennewein DM, et al. The Sol supercomputer at Arizona state university. In: Practice and experience in advanced research computing 2023: computing for the common good (PEARC '23). Association for Computing Machinery; 2023. p. 296–301.
Johnston SE. Understanding the genetic basis of variation in meiotic recombination: past, present, and future. Mol Biol Evol. 2024:41:msae112. https://doi.org/10.1093/molbev/msae112.
Johri P, et al. Recommendations for improving statistical inference in population genomics. PLoS Biol. 2022:20:e3001669. https://doi.org/10.1371/journal.pbio.3001669.
Keeney S. Mechanism and control of meiotic recombination initiation. Cur Top Dev Biol. 2001:52:1–53. https://doi.org/10.1016/S0070-2153(01)52008-6.
Kinzey W. New world primates: ecology, evolution, and behavior. Aldine de Gruyter; 1997.
Kleiman DG. Monogamy in mammals. Q Rev Biol. 1977:52:39–69. https://doi.org/10.1086/409721.
Kolmogorov M, Yuan J, Lin Y, Pevzner PA. Assembly of long, error-prone reads using repeat graphs. Nat Biotechnol. 2019:37: 540–546. https://doi.org/10.1038/s41587-019-0072-8.
Kong A, et al. A high-resolution recombination map of the human genome. Nat Genet. 2002:31:241–247. https://doi.org/10.1038/ng917.
Kong A, et al. Recombination rate and reproductive success in humans. Nat Genet. 2004:36:1203–1206. https://doi.org/10.1038/ng1445.
Kong A, et al. Fine-scale recombination rate differences between sexes, populations and individuals. Nature. 2010:467: 1099–1103. https://doi.org/10.1038/nature09525.
Korhonen J, Martinmäki P, Pizzi C, Rastas P, Ukkonen E. MOODS: fast search for position weight matrix matches in DNA sequences. Bioinformatics. 2009:25:3181–3182. https://doi.org/10.1093/bioinformatics/btp554.
Lenormand T, Dutheil J. Recombination difference between sexes: a role for haploid selection. PLoS Biol. 2005:3:e63. https://doi.org/10.1371/journal.pbio.0030063.
Li H. Aligning sequence reads, clone sequences and assembly contigs with BWA-MEM [preprint]. arXiv. 1303.3997. 2013. https://doi.org/10.48550/arXiv.1303.3997
Li H. Minimap2: pairwise alignment for nucleotide sequences. Bioinformatics. 2018:34:3094–3100. https://doi.org/10.1093/bioinformatics/bty191.
Li R, et al. A high-resolution map of non-crossover events reveals impacts of genetic diversity on mammalian meiotic recombination. Nat Commun. 2019:10:3900. https://doi.org/10.1038/s41467-019-11675-y.
Lorenz A, Mpaulo SJ. Gene conversion: a non-Mendelian process integral to meiotic recombination. Heredity (Edinb). 2022:129: 56–63. https://doi.org/10.1038/s41437-022-00523-3.
Lorenz R, Mason WA. Establishment of a colony of titi monkeys. Int Zoo Yearb. 1971:11:168–174. https://doi.org/10.1111/j.1748-1090.1971.tb01896.x.
Lukas D, Clutton-Brock TH. The evolution of social monogamy in mammals. Science. 2013:341:526–530. https://doi.org/10.1126/science.1238677.
Madeira F, et al. Search and sequence analysis tools services from EMBL-EBI in 2022. Nucleic Acids Res. 2022:50:W276–W279. https://doi.org/10.1093/nar/gkac240.
Martin HC, et al. Multicohort analysis of the maternal age effect on recombination. Nat Commun. 2015:6:7846. https://doi.org/10.1038/ncomms8846.
Masaki N, Browning SR. Modeling the length distribution of gene conversion tracts in humans from the UK biobank sequence data. PLoS Genet. 2025:21:e1011951. https://doi.org/10.1371/journal.pgen.1011951.
Muller HJ. The mechanism of crossing-over. Am Nat. 1916:50: 193–221. https://doi.org/10.1086/279534.
Myers S, et al. Drive against hotspot motifs in primates implicates the PRDM9 gene in meiotic recombination. Science. 2010:327:876–879. https://doi.org/10.1126/science.1182363.
Myers S, Bottolo L, Freeman C, McVean G, Donnelly P. A fine-scale map of recombination rates and hotspots across the human genome. Science. 2005:310:321–324. https://doi.org/10.1126/science.1117196.
Myers S, Freeman C, Auton A, Donnelly P, McVean G. A common sequence motif associated with recombination hot spots and genome instability in humans. Nat Genet. 2008:40: 1124–1129. https://doi.org/10.1038/ng.213.
Neale MJ, Keeney S. Clarifying the mechanics of DNA strand exchange in meiotic recombination. Nature. 2006:442:153–158. https://doi.org/10.1038/nature04885.
Odenthal-Hesse L, Berg IL, Veselis A, Jeffreys AJ, May CA. Transmission distortion affecting human noncrossover but not crossover recombination: a hidden source of meiotic drive. PLoS Genet. 2014:10: e1004106. https://doi.org/10.1371/journal.pgen.1004106.
Oliver PL, et al. Accelerated evolution of the PRDM9 speciation gene across diverse metazoan taxa. PLoS Genet. 2009:5: e1000753. https://doi.org/10.1371/journal.pgen.1000753.
Otto SP, Payseur BA. Crossover interference: shedding light on the evolution of recombination. Annu Rev Genet. 2019:53:19–44. https://doi.org/10.1146/annurev-genet-040119-093957.
Palsson G, et al. Complete human recombination maps. Nature. 2025:639:700–707. https://doi.org/10.1038/s41586-024-08450-5.
Pardo-Manuel de Villena F, Sapienza C. Recombination is proportional to the number of chromosome arms in mammals. Mamm Genome. 2001:12:318–322. https://doi.org/10.1007/s003350020005.
Parvanov ED, Petkov PM, Paigen K. PRDM9 controls activation of mammalian recombination hotspots. Science. 2010:327:835. https://doi.org/10.1126/science.1181495.
Patel A, Horton JR, Wilson GG, Zhang X, Cheng X. Structural basis for human PRDM9 action at recombination hot spots. Genes Dev. 2016:30:257–265. https://doi.org/10.1101/gad.274928.115.
Pfeifer SP. From next-generation resequencing reads to a high-quality variant data set. Heredity (Edinb). 2017:118:111–124. https://doi.org/10.1038/hdy.2016.102.
Pfeifer SP. A fine-scale genetic map for vervet monkeys. Mol Biol Evol. 2020:37:1855–1865. https://doi.org/10.1093/molbev/msaa079.
Pfeifer SP, Baxter A, Savidge LE, Sedlazeck FJ, Bales KL. *De novo* genome assembly for the coppery titi monkey (*Plecturocebus cupreus*): an emerging nonhuman primate model for behavioral research. Genome Biol Evol. 2024:16:evae108. https://doi.org/10.1093/gbe/evae108.
Porsborg PS, et al. Long-read sequencing of primate testis and human sperm allows identification of recombination events in individuals. Nat Commun. 2025:16:10337. https://doi.org/10.1038/s41467-025-65248-3.
Porubsky D, et al. Human *de novo* mutation rates from a four-generation pedigree reference. Nature. 2025:643:427–436. https://doi.org/10.1038/s41586-025-08922-2.

Powers NR, et al. The meiotic recombination activator PRDM9 trimethylates both H3K36 and H3K4 at recombination hotspots in vivo. PLoS Genet. 2016:12:e1006146. https://doi.org/10.1371/journal.pgen.1006146.
Pratto F, et al. Recombination initiation maps of individual human genomes. Science. 2014:346:1256442. https://doi.org/10.1126/science.1256442.
Prentout D, et al. Germline mutation rates and fine-scale recombination parameters in zebra finch. PLoS Genet. 2025:21:e1011661. https://doi.org/10.1371/journal.pgen.1011661.
Quinlan AR, Hall IM. BEDTools: a flexible suite of utilities for comparing genomic features. Bioinformatics. 2010:26:841–842. https://doi.org/10.1093/bioinformatics/btq033.
R Core Team. R: a language and environment for statistical computing. R Foundation for Statistical Computing; 2024. https://www.R-project.org/.
Rice P, Longden I, Bleasby A. EMBOSS: the European molecular biology open software suite. Trends Genet. 2020:16:276–277. https://doi.org/10.1016/S0168-9525(00)02024-2.
Robinson WP, et al. Maternal meiosis I non-disjunction of chromosome 15: dependence of the maternal age effect on level of recombination. Hum Mol Genet. 1998:7:1011–1019. https://doi.org/10.1093/hmg/7.6.1011.
Rogers J, et al. A genetic linkage map of the baboon (*Papio hamadryas*) genome based on human microsatellite polymorphisms. Genomics. 2000:67:237–247. https://doi.org/10.1006/geno.2000.6245.
Rogers J, et al. An initial genetic linkage map of the rhesus macaque (*Macaca mulatta*) genome using human microsatellite loci. Genomics. 2006:87:30–38. https://doi.org/10.1016/j.ygeno.2005.10.004.
San Filippo J, Sung P, Klein H. Mechanism of eukaryotic homologous recombination. Annu Rev Biochem. 2008:77:229–257. https://doi.org/10.1146/annurev.biochem.77.061306.125255.
Sardell JM, Kirkpatrick M. Sex differences in the recombination landscape. Am Nat. 2020:195:361–379. https://doi.org/10.1086/704943.
Schweiger R, et al. Insights into non-crossover recombination from long-read sperm sequencing [preprint]. bioRxiv 602249. 2024. https://doi.org/10.1101/2024.07.05.602249
Ségurel L, Leffler EM, Przeworski M. The case of the fickle fingers: how the PRDM9 zinc finger protein specifies meiotic recombination hotspots in humans. PLoS Biol. 2011:9:e1001211. https://doi.org/10.1371/journal.pbio.1001211.
Shumate A, Salzberg SL. Liftoff: accurate mapping of gene annotations. Bioinformatics. 2021:37:1639–1643. https://doi.org/10.1093/bioinformatics/btaa1016.
Soni V, Pfeifer SP, Jensen JD. Recent insights into the evolutionary genomics of the critically endangered aye-aye (*Daubentonia madagascariensis*). Am J Primatol. 2025a:87:e70105. https://doi.org/10.1002/ajp.70105.
Soni V, Versoza CJ, Jensen JD, Pfeifer SP. Inferring the landscape of mutation and recombination in the common marmoset (*Callithrix jacchus*) in the presence of twinning and hematopoietic chimerism [preprint]. bioRxiv 662565. 2025b. https://doi.org/10.1101/2025.07.01.662565
Soni V, Versoza CJ, Terbot JW, Jensen JD, Pfeifer SP. Inferring fine-scale mutation and recombination rate maps in aye-ayes (*Daubentonia madagascariensis*). Ecol Evol. 2025c:15:e72314. https://doi.org/10.1002/ece3.72314.
Spatola GJ, et al. Comparing fine-scale mutation and recombination landscapes in rhesus macaque (*Macaca mulatta*) populations of Chinese and Indian descent inferred from both short- and long-read sequencing data [preprint]. bioRxiv 727910. 2026. https://doi.org/10.64898/2026.05.26.727910
Stevison LS, et al. The time scale of recombination rate evolution in great apes. Mol Biol Evol. 2016:33:928–945. https://doi.org/10.1093/molbev/msv331.
Sun H, Treco D, Schultes NP, Szostak JW. Double-strand breaks at an initiation site for meiotic gene conversion. Nature. 1989:338:87–90. https://doi.org/10.1038/338087a0.
Terbot JW, et al. Interpreting patterns of X chromosomal relative to autosomal diversity in aye-ayes (*Daubentonia madagascariensis*). Am J Primatol. 2025a:87:e70091. https://doi.org/10.1002/ajp.70091.
Terbot JW, et al. Re-evaluating the demographic history of, and inferring the fine-scale recombination landscape for, wild Chinese rhesus macaques (*Macaca mulatta*). Am J Primatol. 2025b:87:e70088. https://doi.org/10.1002/ajp.70088.
UniProt Consortium. UniProt: the universal protein knowledgebase in 2025. Nucleic Acids Res. 2025:53:D609–D617. https://doi.org/10.1093/nar/gkae1010.
van der Auwera GA, O'Connor BD. Genomics in the cloud: using docker, GATK, and WDL in terra. O'Reilly Media; 2020.
Versoza CJ, et al. Novel insights into the landscape of crossover and noncrossover events in rhesus macaques (*Macaca mulatta*). Genome Biol Evol. 2024:16:evad223. https://doi.org/10.1093/gbe/evad223.
Versoza CJ, Bales KL, Jensen JD, Pfeifer SP. The landscape of structural variation in coppery titi monkeys (*Plecturocebus cupreus*) [preprint]. bioRxiv 699302. 2026. https://doi.org/10.64898/2026.01.13.699302
Versoza CJ, Lloret-Villas A, Jensen JD, Pfeifer SP. A pedigree-based map of crossovers and noncrossovers in aye-ayes (*Daubentonia madagascariensis*). Genome Biol Evol. 2025:17:evaf072. https://doi.org/10.1093/gbe/evaf072.
Versoza CJ, Pfeifer SP. A hybrid genome assembly of the endangered aye-aye (*Daubentonia madagascariensis*). G3 (Bethesda). 2024:14:jkae185. https://doi.org/10.1093/g3journal/jkae185.
Wall JD, Robinson JA, Cox LA. High-resolution estimates of crossover and noncrossover recombination from a captive baboon colony. Genome Biol Evol. 2022:14:evac040. https://doi.org/10.1093/gbe/evac040.
Wang K, Li M, Hakonarson H. ANNOVAR: functional annotation of genetic variants from high-throughput sequencing data. Nucleic Acids Res. 2010:38:e164. https://doi.org/10.1093/nar/gkq603.
Wang S, Zickler D, Kleckner N, Zhang L. Meiotic crossover patterns: obligatory crossover, interference and homeostasis in a single process. Cell Cycle. 2015:14:305–314. https://doi.org/10.4161/15384101.2014.991185.
Webb AJ, Berg IL, Jeffreys A. Sperm cross-over activity in regions of the human genome showing extreme breakdown of marker association. Proc Natl Acad Sci U S A. 2008:105:10471–10476. https://doi.org/10.1073/pnas.0804933105.
Wijnker E, et al. The genomic landscape of meiotic crossovers and gene conversions in *Arabidopsis thaliana*. Elife. 2013:2:e01426. https://doi.org/10.7554/eLife.01426.
Williams AL, et al. Non-crossover gene conversions show strong GC bias and unexpected clustering in humans. Elife. 2015:4:e04637. https://doi.org/10.7554/eLife.04637.
Xue C, et al. The population genomics of rhesus macaques (*Macaca mulatta*) based on whole-genome sequences. Genome Res. 2016:26:1651–1662. https://doi.org/10.1101/gr.204255.116.
Xue C, et al. Reduced meiotic recombination in rhesus macaques and the origin of the human recombination landscape. PLoS One. 2020:15:e0236285. https://doi.org/10.1371/journal.pone.0236285.

Associate editor: Adam Eyre-Walker